J. Space Weather Space Clim. 2023, **13**, 14
© G. Koban et al., Published by EDP Sciences 2023
https://doi.org/10.1051/swsc/2023011

JSWSC
Available online at:
www.swsc-journal.org

Research Article Open Access

Orientation of the stream interface in CIRs

Gergely Koban[1,2,*], Andrea Opitz[1], Nikolett Biro[1,2], and Zoltan Nemeth[1]

[1] Wigner Research Centre for Physics, Konkoly-Thege Miklos street 29-33, 1121 Budapest, Hungary
[2] Eötvös Loránd University, Doctoral School of Physics, Pázmány Péter walkway 1/A, 1117 Budapest, Hungary

Received 10 November 2022 / Accepted 14 April 2023

Abstract – Corotating Interaction Regions (CIRs) are complex structures in the Heliosphere that arise from the interaction of fast and slow solar wind streams. The interface between fast and slow solar wind is called the stream interface, which often has considerable north-south tilt. We apply a sliding window correlation method on multi-spacecraft data in order to obtain the time delay between the spacecraft. Using these time delays and in-situ solar wind velocity measurements, we can shift the positions of two spacecraft, and, together with the position of the reference spacecraft, we can reconstruct the spatial orientation of the stream interface. We examined four CIRs from two different solar sources at the beginning of 2007 using ACE, WIND, and STEREO-A spacecraft data. The gradually increasing distance between STEREO-A and the other spacecraft provides an opportunity to determine the effects of spacecraft separation on the quality of the results. In three out of the four events, the determined planes generally follow the Parker spiral in the ecliptic, their off-ecliptic tilt is determined by the position of the source of the high-speed stream. For the fourth event, STEREO-A was probably too far away for this method to be successfully applied.

Keywords: Corotating interaction regions / Solar wind

1. Introduction

As a first approximation, there are two significantly different types of the solar wind, namely the fast and the slow solar wind. The differences between the two types are not limited to the plasma velocity, some of their other properties (e.g., temperature, density, and composition) also differ notably. The general understanding is that fast solar wind originates from coronal holes (Phillips et al., 1995; Neugebauer, 1999), while the source of the slow solar wind is less clear. According to Richardson (2018), the main source for slow streams is the streamer belt over the equatorial regions of the Sun while Wang et al. (2000) find that it comes from small coronal holes, the edges of larger holes, and/or from the streamer region.

Coronal holes are low-density regions in the solar corona, cooler than their surroundings. Magnetic field lines originating from coronal holes are open, and they extend out to interplanetary space. Although coronal holes can develop at any time on the corona of the Sun, they are more persistent during solar activity minimum, and they can last through several solar rotations. Generally speaking, they are the source of fast and low-density solar wind observed in interplanetary space. Bagashvili et al. (2017) studied coronal holes in the time period ranging from 1 January 2013 to 20 April 2015 and found that fast streams have a recurrence rate matching the synodic rotation period of the Sun, i.e. around 28 days. The interaction of fast and slow solar wind streams during their radial propagation plays a dominant role in determining the structure of the heliosphere.

Stream Interaction Regions (SIRs) are structures in the solar wind that form when fast solar wind streams (originating from coronal holes) catch up with slow solar wind streams. After completing a solar rotation, we call them Corotating Interaction Regions (CIRs). Radially aligned slow and fast solar wind plasma streams constitute different plasma regimes since they originate from different positions on the rotating Sun and at different times. According to Alfven's theorem, this fact prevents the faster solar wind from penetrating and taking over the slower stream. In a virtual collision-free environment, where the resistance-free ideal form of the induction equation is satisfied, the plasma originally situated inside a given flux tube must remain there, and thus flux tubes originating from different plasma regimes cannot mix (Richardson, 2018). In other words, the increasing plasma and magnetic pressure prevent the fast stream from taking over the slow stream. Their interaction forms a compression zone with density and temperature enhancement in the solar wind along the interaction surface. The interface between fast and slow solar wind is called the stream interface (SI) (Burlaga, 1974), and mature CIRs often produce forward shocks at the leading edge and reverse shocks at the trailing edge. The SI separates the slow, dense plasma from the fast and tenuous plasma, and as such, it is associated

*Corresponding author: koban.gergely@wigner.hu

with a pressure peak and shear in the flow. The formation of CIRs starts in the inner heliosphere, and they are typically well-formed near the Earth's orbit, at 1 AU. The stream interface of CIRs can have considerable tilt in the north-south axis (Gosling & Pizzo, 1999). Studying these tilts and the spatial structure of the stream interface is important because they can give us insight into the conditions of the Sun (see e.g., Simunac et al., 2009).

In this paper, we attempt to determine the local geometry of the stream interface in three dimensions. As with every smooth surface, the CIR stream interface also can be approximated by its tangent plane locally. Properties of this tangent plane can be computed if we can determine at least three relatively closely spaced points of the SI. The points cannot be too far for the linear approximation to be still adequate (a few million km at maximum) but cannot be too close either (we estimate at least a few tens of thousands of km), because in that case, the uncertainties of the position determination could lead to large errors in the computed plane parameters. One purpose of this paper is to gain more profound knowledge about the effects of spacecraft separation on the applicability of this technique. The method requires at least three spacecraft, relatively close to each other.

We worked in the Heliocentric Earth Ecliptic coordinate system (Hapgood, 1992). Its X axis points towards the Earth from the Sun, while its Z axis is perpendicular to the plane of Earth's orbit around the Sun, with the positive direction pointing North. All ephemeris and measurement data were obtained from the AMDA database and tool (Génot et al., 2021), except for the ephemeris data of STEREO-A, which were obtained from the Caltech website.

For our current study, we chose the beginning of 2007 because, during this time period, there were two CIRs per solar rotation. Opitz et al. (2014) have identified eight CIRs over the course of four months starting from February 2007. Furthermore, a CIR list for 2007 is available in Mason et al. (2009). At the start of the year, WIND (Harten & Clark, 1995) and ACE (Stone et al., 1998) were in the L1 point, while STEREO-A (Kaiser et al., 2008) was also nearby, but accelerating away from the Earth after a lunar flyby on 15th December 2006. The distance between the ACE probe and the Sun increases steadily between *0.974* AU and *0.981* AU during the course of these two months, while the distance between the STEREO-A and the Sun decreases from *0.975* AU to *0.967* AU. The spatial separations between the probes changed on the scale of a few hundred thousand km to a few million km. On the HEE z-axis (latitude), the greatest separation was ~350,000 km near the 10th of January with ACE and WIND moving close to each other (around 10,000 km) and STEREO-A being the one further away from the other two. This changes over the course of the month, with both ACE and WIND crossing over the ecliptic (HEE $z = 0$), and STEREO-A is moving closer to it, but they still keep a separation of 150,000 km along the HEE z-axis. In terms of overall distance between ACE and STEREO-A, it is around 900,000 km at the beginning of January and steadily grows – by the time of the last event, 25th February, it reaches 3.5 million km. As a result, STEREO-A traveled too far away from the other two spacecraft for the purposes of this study from March 2007 on, so we restricted our time frame to January and February 2007. This situation makes it possible for us to test the limits of the method in terms of spatial separation between the probes. There were four CIRs related to high-speed streams originating from two different coronal holes during these two months. In Figure 1, we marked these four CIRs on velocity, proton density, total magnetic field, temperature, and ram pressure time series recorded by the ACE probe.

2. Method

On large spatial scales, the geometry of CIRs resembles a Parker spiral. On smaller scales, the curve of the stream interface is so small, that it can be considered a plane. We attempt to determine the normal vector of this plane.

Various methods are known to determine the approximate geometry of structures sweeping through a fleet of spacecraft. In previous works, multispacecraft observations were used to identify shock normals (Szabo, 2005) and even magnetic clouds (Kilpua et al., 2009). If we have four spacecraft and need to determine the shock normal, the first step is to identify in the measurement data the time when the shock reached each space probe. After that, using one of the probes as a reference, the time delay for the three remaining spacecraft is determined. Using the known time delays and spatial separations, the shock normal can be calculated according to the following formula (Russell et al., 1983):

$$\begin{pmatrix} \Delta \boldsymbol{X}_1 \\ \Delta \boldsymbol{X}_2 \\ \Delta \boldsymbol{X}_3 \end{pmatrix} \begin{pmatrix} N_x \\ N_y \\ N_z \end{pmatrix} = V \begin{pmatrix} \Delta t_1 \\ \Delta t_2 \\ \Delta t_3 \end{pmatrix}, \tag{1}$$

where the elements of matrix $\boldsymbol{\Delta X}$, the $\boldsymbol{\Delta X_i}$ vectors are the spatial separations in any three-dimensional orthogonal coordinate system between each of the three spacecraft and the reference spacecraft, the elements of $\boldsymbol{\Delta t}$, Δt_i are the corresponding time delays, N_i is the components of the normal vector and V is the speed. This equation can be solved for $(1/V)$ $(\mathbf{N})$. The advantage of this method is that it does not require any former knowledge about the speed V. Since V is a scalar and $\mathbf{N}$ is a unit vector ($\mathbf{N}^2 = 1$), the direction (or the normalized form) of the solution gives the normal vector of the plane. The method we utilized works similarly, but uses the measured solar wind speed, and thus requires one spacecraft less. This means that we have one reference spacecraft, and two spacecraft that we need to shift, using the time delays together with the in-situ solar wind velocity measurements made by these spacecraft.

First, the stream interfaces were identified in the measurements for each CIR by eye. For this purpose, we used measurements of the bulk speed, density, total magnetic field, temperature, and pressure. The characteristic properties of stream interfaces and a routine to identify them in time series were introduced by Burlaga (1974). According to this routine, to identify the stream interface, we should note a sharp decrease in density, and a sharp increase in temperature, while the solar wind velocity continuously increases. Most times an increase in a total magnetic field is also present, but it is not a general characteristic of stream interfaces. We actually utilized five solar wind measurements: bulk velocity, density, total magnetic field, temperature, and pressure. We used the measurements of

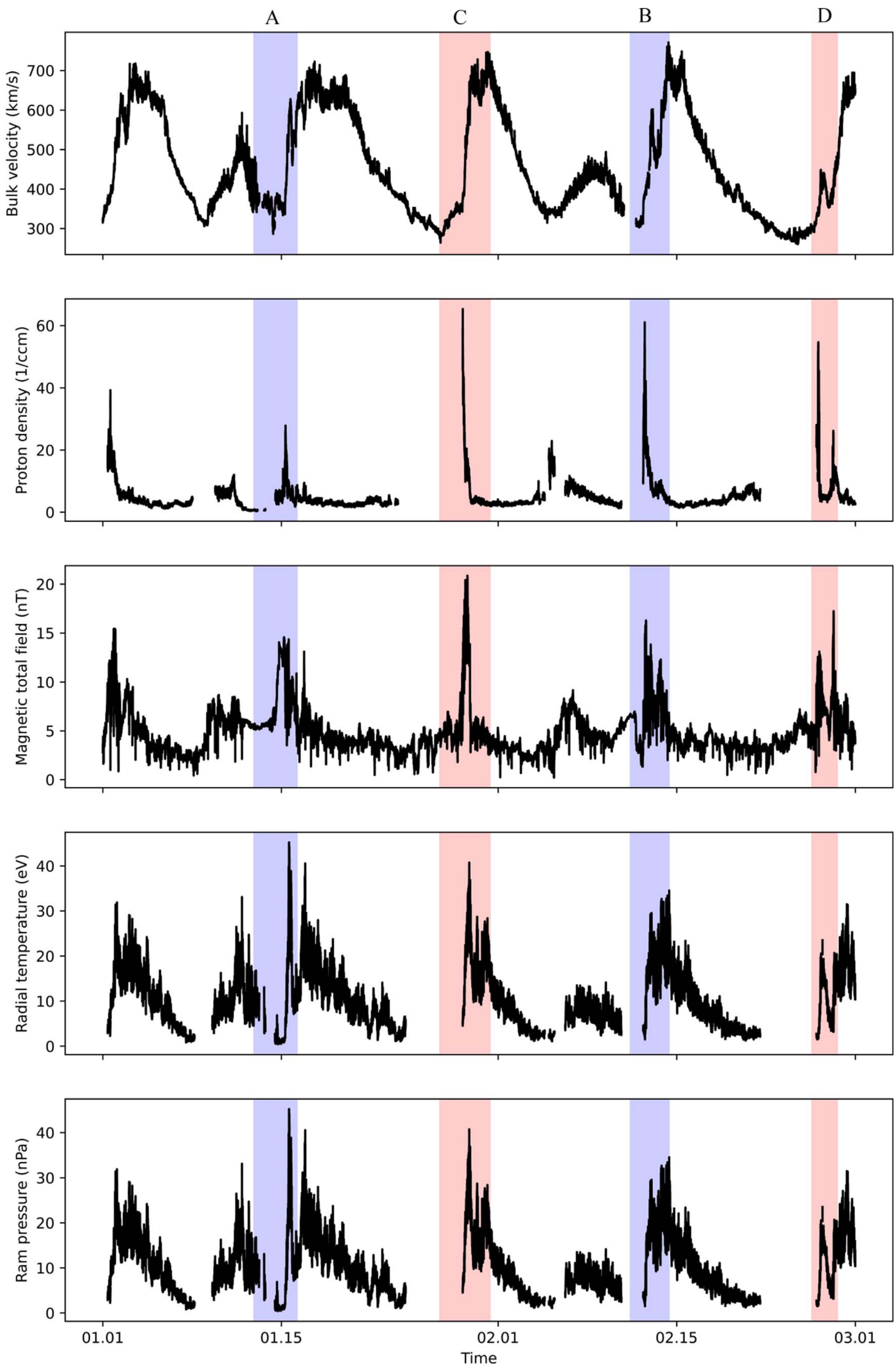

Figure 1. ACE bulk velocity, proton density, total magnetic field, proton radial temperature, and ram pressure data for the 1st January – 1st March 2007 time period. The CIRs studied in this paper are highlighted with shaded background and marked with letters A–D, where A and B originate from the same solar coronal hole (marked with blue), and C and D originate from another coronal hole (marked with red).

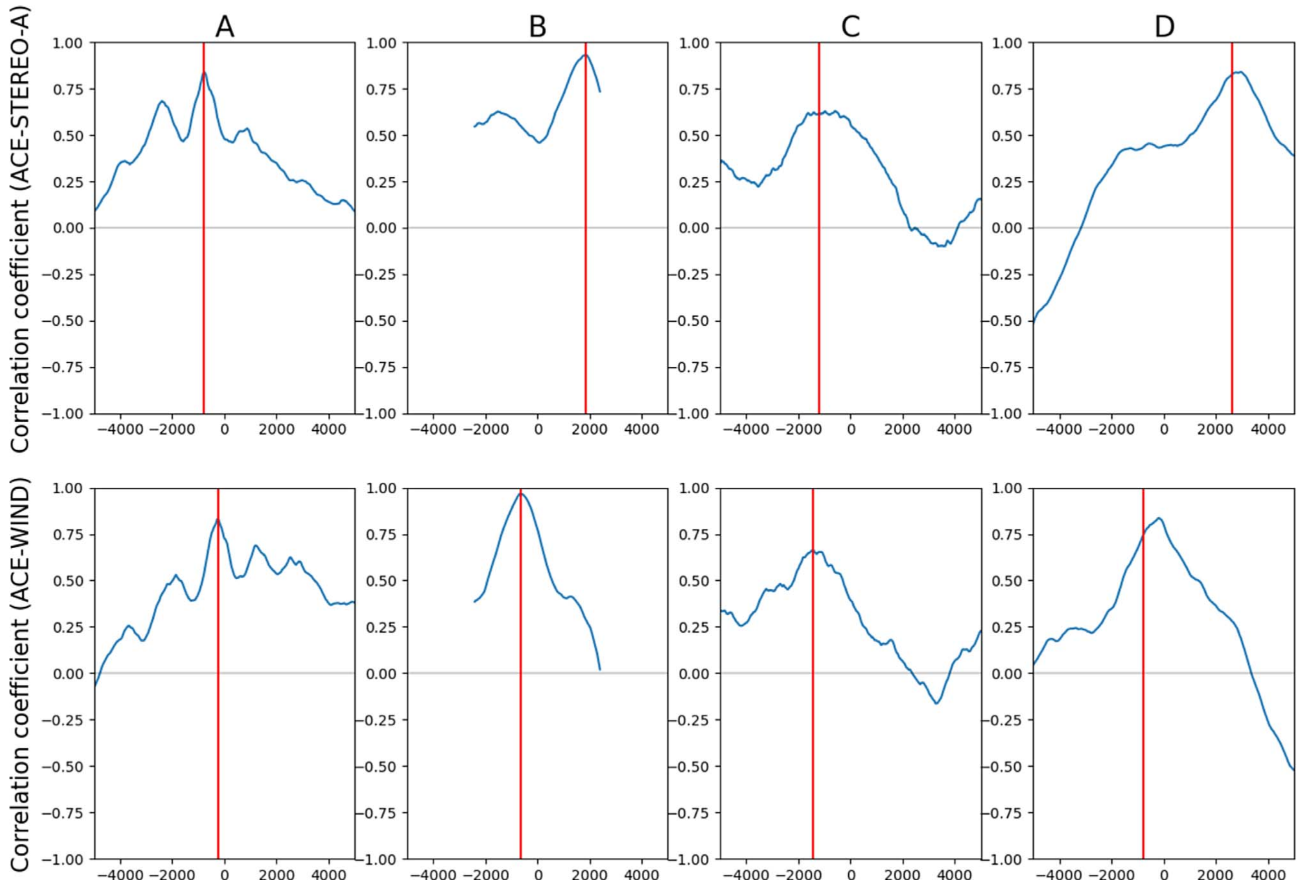

Figure 2. Magnetic field magnitude correlation functions between ACE-STEREO-A and ACE-WIND for all four events. The *x*-axis shows the time delay in seconds. The red vertical lines represent the position of the chosen time delay values, which are: A: STA: −768 s, WIND: −231 s; B: STA: 1860 s, WIND: −651 s; C: STA: −1239 s, WIND: −1449 s; D: STA: 2640 s, WIND: −780 s.

the SWEPAM (McComas et al., 1998) and MAG (Smith et al., 1998) instruments of ACE, the PLASTIC (Galvin et al., 2008), SWEA (Sauvaud et al., 2008), MAG (Acuña et al., 2008) and SEPT (Müller-Mellin et al., 2008) instruments of STEREO-A, and the SWE (Ogilvie et al., 1995) and MFI (Lepping et al., 1995) instruments of WIND.

After we obtained the approximate times for when the stream interface passed the spacecraft, we computed correlation functions of the time series of the total magnetic field between spacecraft pairs. In all three probes, out of all the solar wind parameters, magnetic field data have the best time resolution, so it is most suitable for the purpose of determining the time delays. The three probes have different time resolutions for magnetic field data: STEREO-A is the best with 1 s, then WIND with 3 s, and the ACE has a 16 s resolution. We used 3 s time resolution, so we only needed to use interpolation in one case (ACE). The interpolation was done by AMDA. We used sliding window Pearson correlation around the approximate time of the stream interface, with the ACE probe as a reference. The goal was to determine the time we need to shift the time series of STEREO-A and WIND to have the maximal correlation coefficient with the ACE data. For the first three events, we relied on only the location of the maximum correlation coefficient for magnetic field data, while for the fourth event, we had taken into account correlation results from other datasets. This method gives us a more precise time delay than identification (by eye) of the not-always well-defined SI structure from lower-resolution plasma data. We tried different window sizes for the correlation, between 2 h and 8 h, stepping within 30 min. We found that any 2–4 h long window is sufficient, and that window size does not alter the results significantly. In most cases, the maximum of the correlation coefficient agreed well with the amount we would shift the data by hand, which gives us confidence in the method. In the case of the last CIR at the end of February 2007 (D), using the time delays obtained from the correlation function gave results in the X-Z projection that was obviously wrong. In this case, we needed other considerations to find the actual time delay. A careful analysis of other time series (above all, the density) was required.

Considering how close the probes are to each other, the correlation coefficient is expected to peak at relatively high values. In an ideal setup, the shifted measurements should be nearly identical, as the variations in the solar wind are small on this spatial scale. Of course, we are using different probes with different instruments, different calibrations, and different ages. All things considered, even with the best shifts, there should be differences between the measurements thanks to instrumental errors and small variations in the solar wind. In Figure 2, we can see the correlation coefficients for the time delays between ACE and STEREO-A, and between ACE and WIND for all four events. For event A, we can see a kind of periodicity,

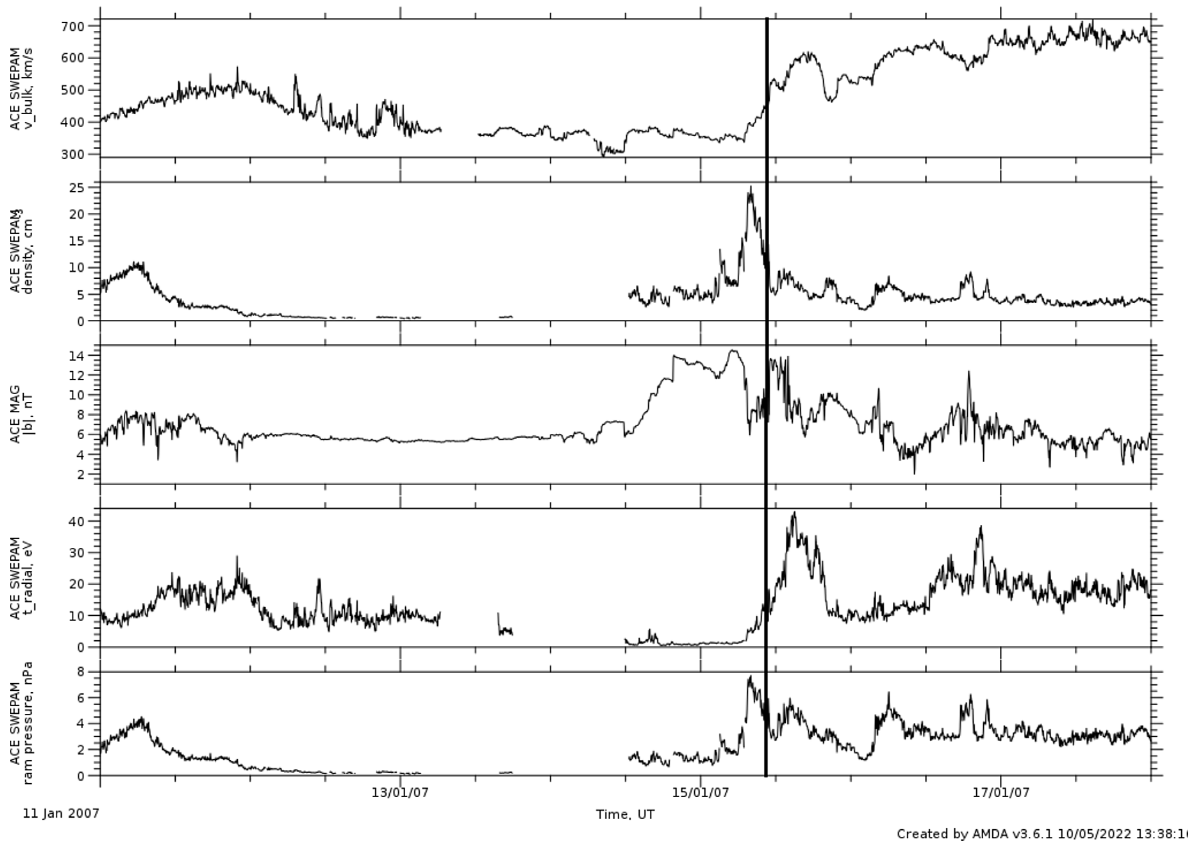

Figure 3. ACE data obtained between January 11 and 18th January 2007 (A). Time is on the x-axis, from 11th to 14th February 2007. On the y-axis are (from top to bottom): the solar wind bulk velocity, proton number density, magnetic total field, radial temperature, and ram pressure. The heavy vertical line refers to the presumed position of the Stream Interface.

the time between two peaks being approximately 30 min. Careful examination of the magnetic field data reveals quasi-periodic variation (sudden depressions) in the field magnitude of all three probes (see Fig. 4). The periodicity of the peaks is caused by these depressions dominating the determination of the correlation. In Figure 2, event C, we can notice a broad "plateau", especially regarding the ACE-STEREO-A correlation. This is most likely caused by local magnetic fluctuations that flatten the peak. The shifted total magnetic field data series for this event can be seen in Figure 6.

The last step was to determine the positions of the three points of the SI plane at the time when the SI passed the ACE spacecraft. One of these points is obviously the position of ACE, the other points can be determined using the positions of the other spacecraft, the solar wind speed, and the time delays determined above. We need to shift the positions of the other two spacecraft according to the delays along the solar wind direction and by the amount determined by the solar wind velocity. For this, we used the solar wind velocity vector measured locally on-board each of the probes. The vector with which to shift the positions is:

$$\Delta \boldsymbol{r} = \boldsymbol{V}_{\mathbf{SW}} \times \Delta t, \tag{2}$$

where Δt is the time delay and $\boldsymbol{V}_{\mathbf{SW}}$ is the solar wind velocity vector. It is important to note that Δt is signed according to the temporal sequence of the events. Unfortunately, STEREO-A velocity measurements began only in the second half of February, before that, we used solar wind velocity measurements performed by WIND for both spacecraft for the calculation. We compared ACE and WIND velocity measurements, and we found that the difference is usually a few percent

After performing the shifts, we have three points: the position of ACE and the shifted positions of STEREO-A and WIND. These three points lie in the plane of the SI. The normal vector of the plane can be computed as the cross product of two vectors pointing from one of the points to the other two. With a point on the plane and the normal vector, the plane is fully determined. For easier comparison, we provide the 2D projections on the X-Y, X-Z, and Y-Z planes for each event. We also calculated the uncertainties using the statistical error of the Pearson correlation. Following Bowley (1928), the formula for the error is:

$$\sigma_r = \sqrt{\frac{1 - r^2}{n - 2}}, \tag{3}$$

where r is the calculated correlation coefficient, and n is the sample size (in our case, the window size). When we have this error, we find the elements on the two sides of the peak corresponding to $r - \sigma_r$. This means that the temporal uncertainty is asymmetric and depends on the slopes leading up to the peak. As a last step, we calculate the normal vector of two additional planes: one defined by the position of ACE and

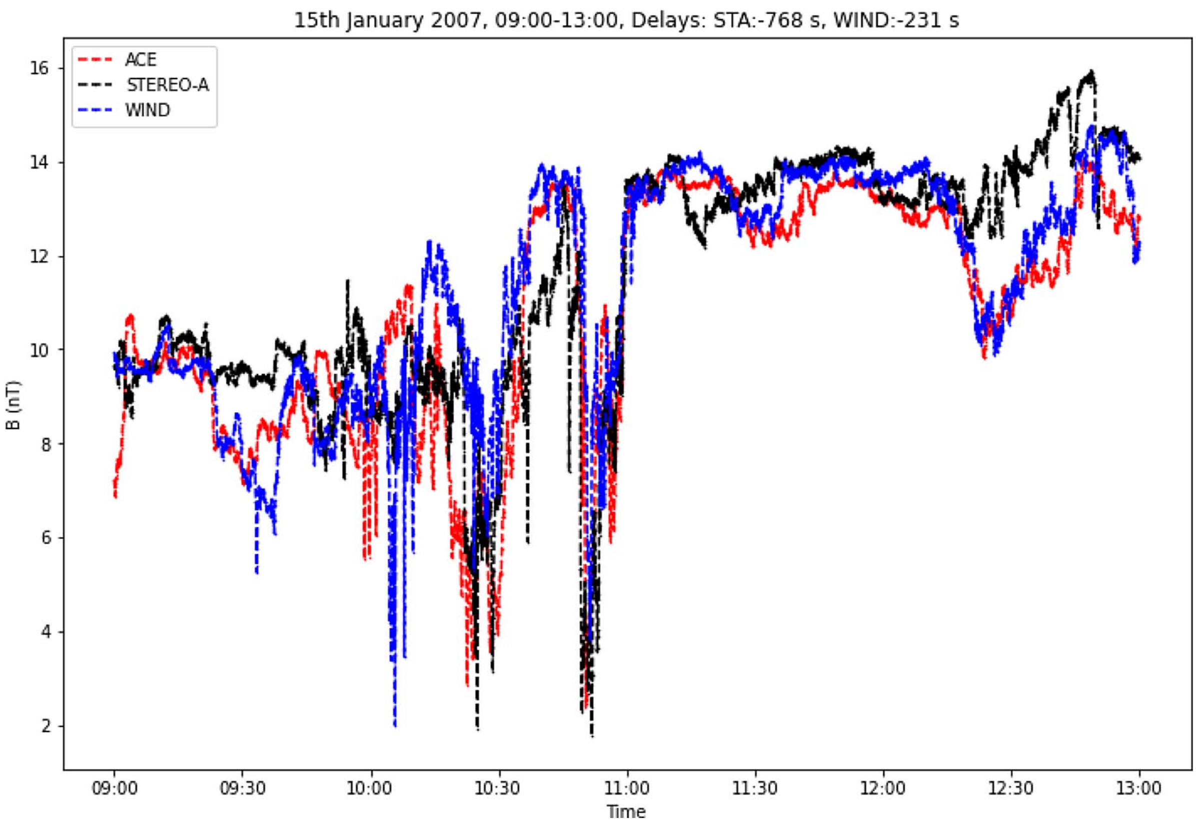

Figure 4. Shifted time series of the total magnetic field measurements for ACE, STEREO-A, and WIND. For the *x*-axis, we used the time of the reference spacecraft, ACE.

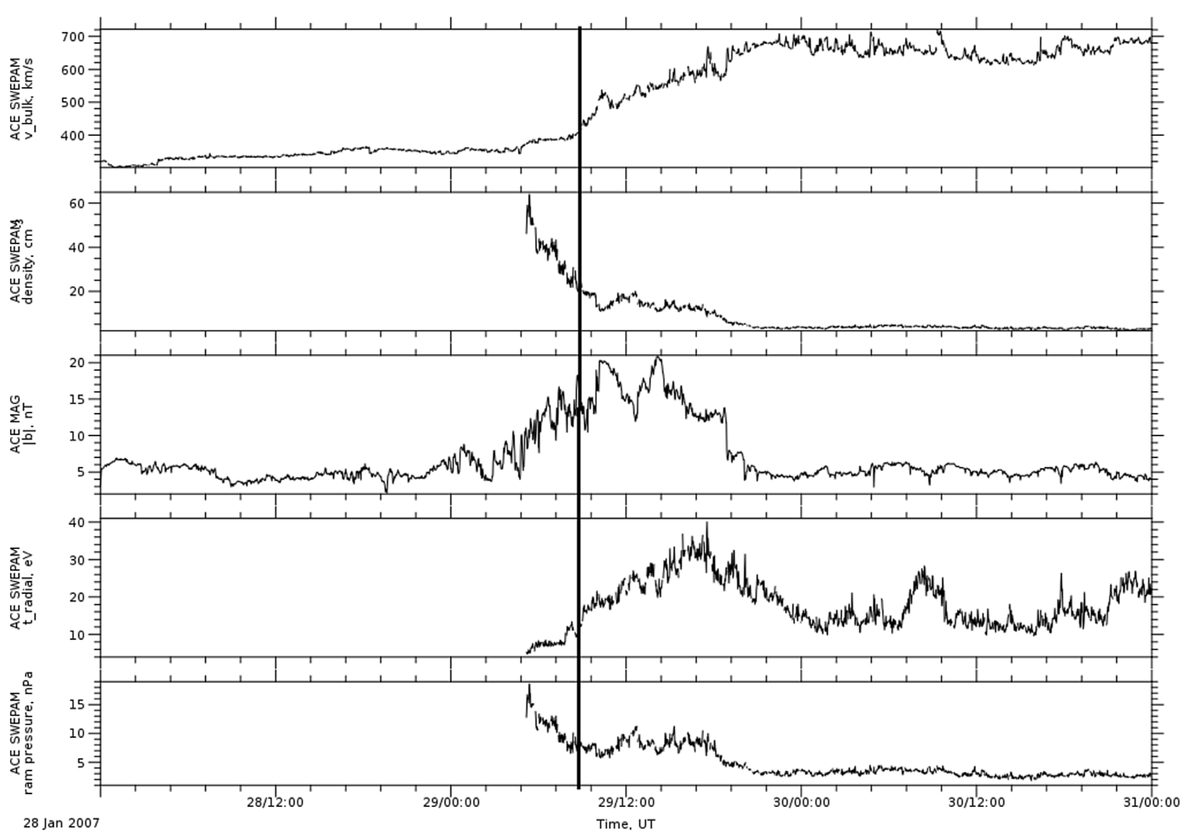

Figure 5. Similar to Figure 3, but for the time period between 28 and 31st January 2007 (C).

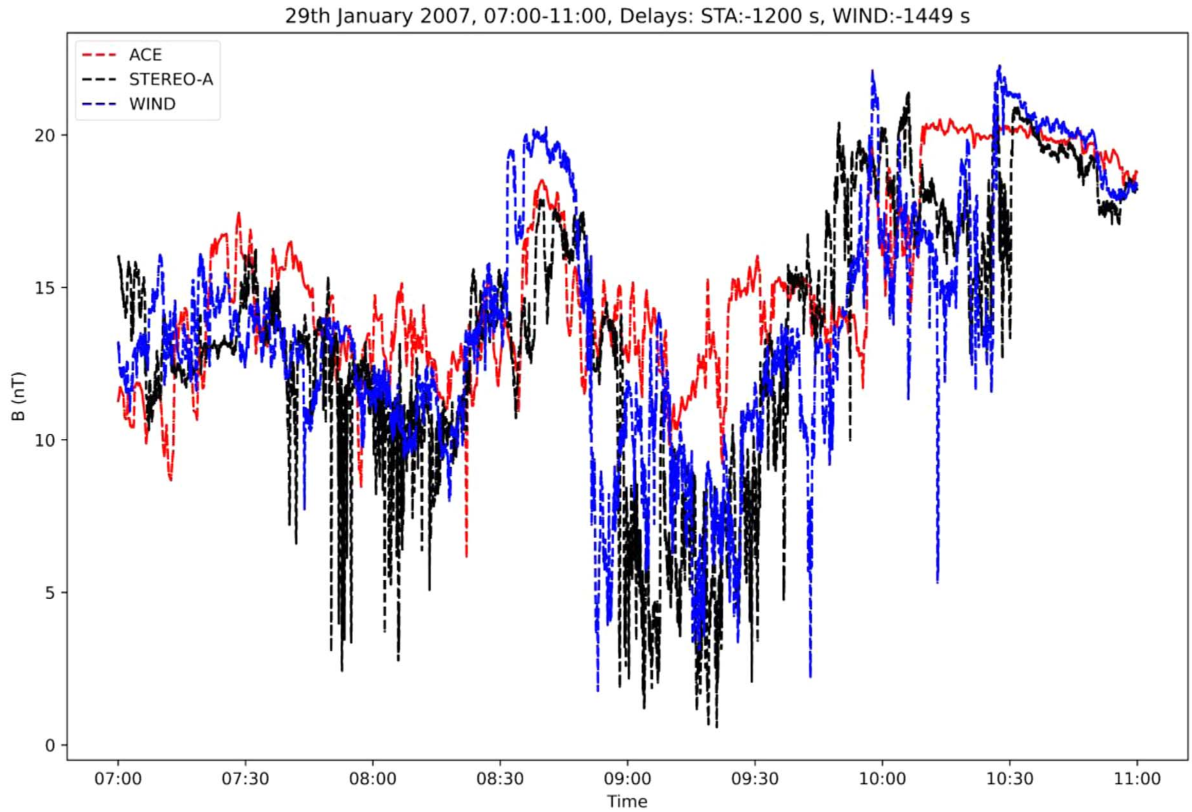

Figure 6. Shifted time series of the total magnetic field measurements for ACE, STEREO-A, and WIND.

Table 1. Errors in correlation and temporal delay determinations.

Event	Spacecraft	Corr. coefficient	Corr. error	Temporal delay (s)	Min. and Max. temporal delays (s)
A	STEREO-A	0.8397	0.00784	−768	[−804, −732]
	WIND	0.8308	0.00804	−231	[−288, −207]
B	STEREO-A	0.9328	0.00520	1860	[1764, 1908]
	WIND	0.9676	0.00364	−651	[−693, −570]
C	STEREO-A	0.6207	0.01109	−1200	[−1434, −480]
	WIND	0.6640	0.01079	−1449	[−1539, −1107]

the positions of WIND and STEREO-A shifted with the minimum possible time delays, while the other consists of the position of ACE and the positions of WIND and STEREO-A shifted with the maximum possible time delays. We also show the projections of these planes next to the original SI planes. The calculated statistical and temporal errors can be seen in Table 1.

3. Results

In this section, we provide case studies of several CIR crossing events and determine the approximating planes of the CIR stream interfaces.

3.1 14–16th January 2007 CIR (A)

The stream interface was identified to be at around 11:00 on the 15th of January. At that time, there is a substantial drop in the density and a sudden increase in the temperature. This can be seen in Figure 3. The data of all three probes show very similar behavior around the SI, meaning we see nearly identical structures in the time series of all probes.

As the next step, we correlated the magnetic field measurements for the 09:00–13:00 h window to obtain the time delays. Both correlation functions had clear peaks. For the STEREO-A probe, the obtained time delay was −768 s with a correlation coefficient value of *0.8397*, and for WIND, it was −231 s with a value of *0.8308*. The results of the shifts can be seen in Figure 4.

ACE and WIND measurements seem to overlap very well, and in the middle area (around 10:00 to 11:00), STEREO-A also follows the pattern of the other two probes. The only differences are the drops around 09:30 and 12:30 which can be seen on both ACE and WIND, but not on STEREO-A. Nevertheless, we achieved a good correlation and obtained the time delays.

Unfortunately, STEREO-A did not have any velocity measurements for this time period, so we had to use the solar wind velocity vector measured by WIND for both spacecraft. The solar wind velocity vector in the HEE coordinate system

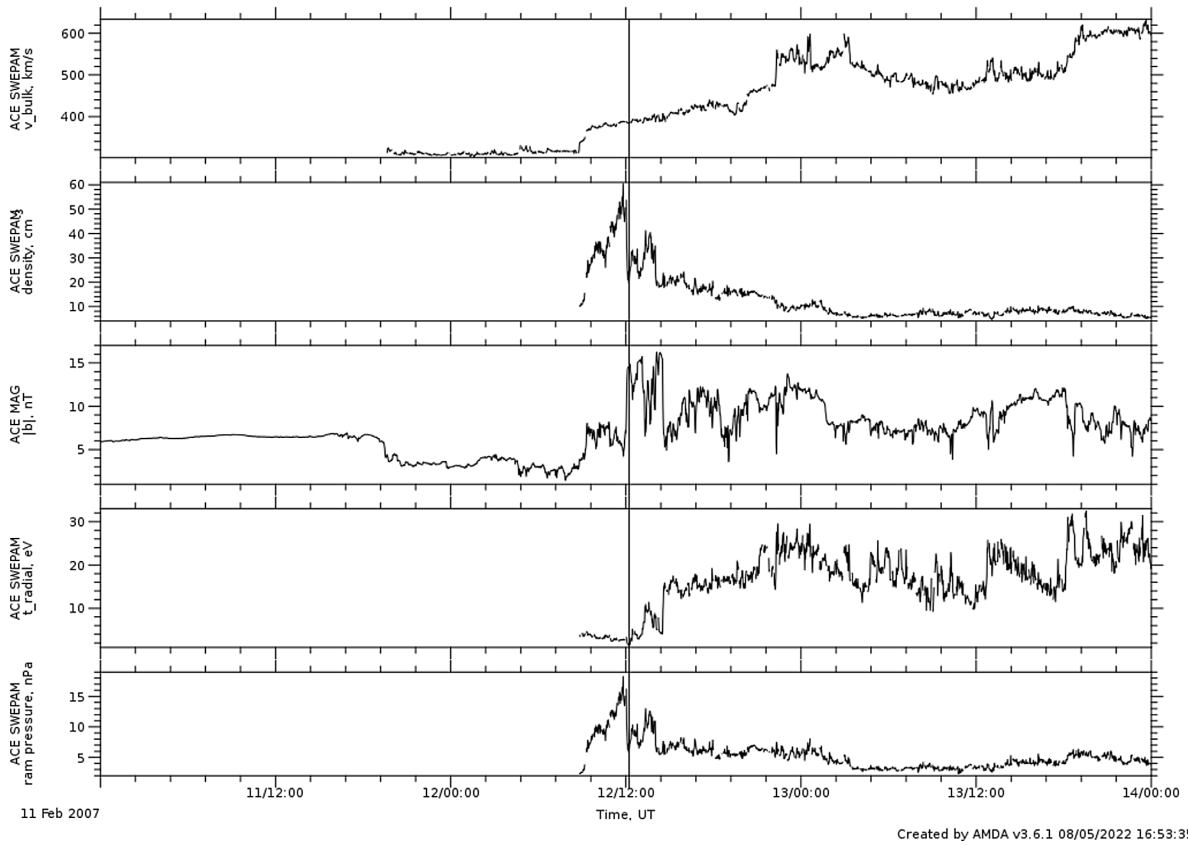

Figure 7. Similar to Figure 3, but for the time period between 11 and 14th February (B).

is (*473.2, 2.9, 47*), where all values are in km/s. Using this vector and time delays, we determined the three points on the plane according to equation (2) and acquired the plane's normal vector. The normal vector was calculated to be (*0.6514, 0.7476, 0.1293*). The three-dimensional structure for event A can be seen in the Supplementary Video. We also calculated the clock and cone angles associated with this vector; the clock angle is: $\theta = \arctan(-M_y/M_z)$ and the cone angle is $\varphi = \arccos(-M_x)$, where M_x, M_y, M_z are the components of the normal vector. In this case, $\varphi = 130.6°$ and $\theta = -80.19°$.

3.2 28–31st January 2007 CIR (C)

In regards to this second event, we placed the Stream Interface to be at around 29th January 2007, 09:00. As we can see in Figure 5, there is a slight drop in proton density, and nearly at the same time, a more significant increase in the temperature at that time.

Then the correlation functions of the total magnetic field measurements were obtained for the time window 07:00–11:00 on the same day. The correlations had clear peaks which matched the time shift we would expect to come to by eye, although the peaks were somewhat lower this time. The peak for STEREO-A was at −1200 s, with the value *0.6207*. For WIND, it was at −1449 s, with a value of *0.6640*.

We can see in Figure 6, that there are some significant differences in the measured total magnetic field at this time between the probes, which likely causes the relatively low correlation coefficient peak. Nevertheless, characteristic points like the peak around 08:30, and the main slopes align well.

We used the WIND solar wind velocity data for STEREO-A, too, in absence of its own measurements. The solar wind velocity vector was *(401, 65, 5),* with all units in km/s. Using this solar wind vector, we obtained the positions where the probes encountered the plane of the stream interface according to the method presented in the previous chapter. The normal vector of the plane was calculated to be *(0.5539, 0.7672, 0.3231). The cone angle* $\varphi = 123.6°$ *and the clock angle is* $\theta = -67.16°$.

3.3 11–14th February 2007 CIR (B)

For this event, we identified the Stream Interface to be around 12th February 2007, 12:02. All the unique identifying marks of the stream interface are present at this time, as we can see in Figure 7.

Although there is a more substantial increase in the temperature a little later, around 14:00, it does not line up with the density drop above it exactly.

Next, we correlated the total magnetic field measurements for the time window 10:00–14:00. The correlations had clear peaks. For STEREO-A, the peak was at 1860 s, with a value of *0.9328*, while for WIND, it was at −651 s, with a value of *0.9676*. We can see the results after the shift in Figure 8.

As we can see, the measurements line up well and the major variations overlap. There are some differences of course, most notably the sudden depression around 10:30 in the STEREO-A data, which is not present at any other probes.

Once again, we had to use the WIND solar wind vector measurements for both spacecraft. The velocity in the HEE

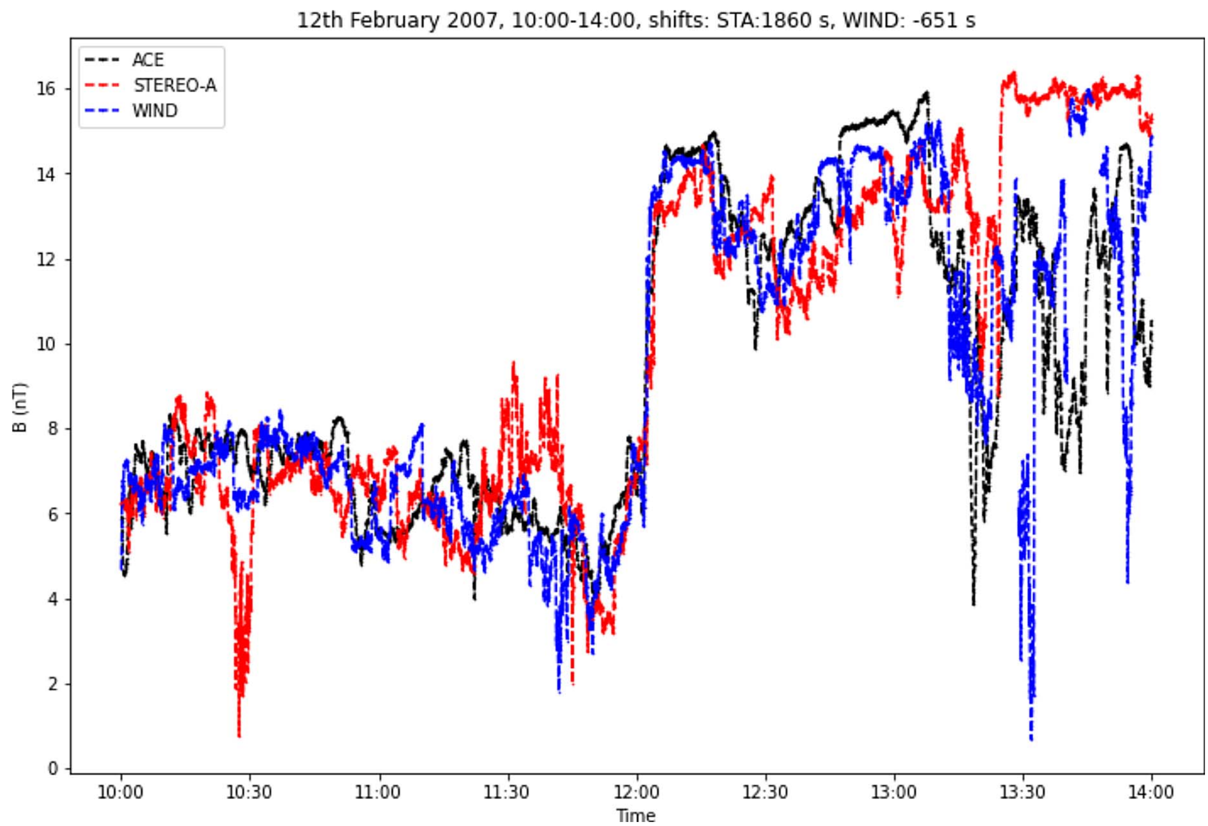

Figure 8. Shifted time series of the total magnetic field measurements for ACE, STEREO-A, and WIND.

coordinate system is: *(391, 25, −9)*. All values are in km/s. The normal vector of this plane was calculated to be *(0.9574, 0.2841, 0.0511). The calculated angles are* φ *= 163.2° and* θ *= −79.8°.*

3.4 25–28th February 2007 CIR (D)

For this event, STEREO-A was significantly farther away from the other two spacecraft. This fact and certain attributes of this CIR made it more difficult to obtain the offsets in this case.

The data indicated that the Stream Interface is around 27th February 2007, 07:00. As can be seen in Figure 9, a relatively small, but clear drop in density and a much more significant increase in temperature are present at that time.

In Figure 9, we can see that this event is no ordinary CIR; there are double peaks in all five parameters, likely indicating the interference of another solar wind structure. We can see the peaks where we placed the stream interface, and there are peaks just a few hours before that, most notably in density, magnetic field, and ram pressure data. In this case, using just the magnetic field data resulted in a horizontal (lying in the *x–y* plane) SI plane, which is very unlikely: such a situation would require an unphysically large latitudinal velocity gradient. We could not rely only on the magnetic field measurements this time: we used other data (especially the density) to correct our determined offsets, because introducing other datasets may help balance out the interfering effects of local fluctuating effects. Figure 10 shows the correlation between the probes for this event. For the correlation between the ACE and STEREO-A, there was a peak with a ~7 min wide "plateau", which made it difficult to obtain the right offset from the correlation function. As for the WIND correlation, although it gave a clear peak, the other data did not support the obtained offset. We had to adjust the shifts in accordance with the density data. Our best-obtained shift for the density measurements can be seen in Figure 12. Although there were significant differences between the data recorded by the ACE-WIND pair and that of STEREO-A (most likely due to the large distance between them), we can see that the shifted time series mostly move together, especially in the central area of the plot.

The final time delays are 2640 s with a correlation coefficient value of *0.8287* for STEREO-A, and −780 s with a correlation value of *0.7447* for WIND. In contrast, the maximum correlation values (from only the magnetic field data) were *0.8401* and *0.8366* for STEREO-A and WIND, respectively. The result of the final shifts can be seen in Figure 11.

At this time, the STEREO-A already had solar wind velocity measurements. The velocity vectors in HEE were determined to be the following: STEREO-A: (*445, 0, 28*), WIND: (*454, −2, 37*). The normal vector of the plane was calculated to be *(−0.6561, −0.2245, −0.7204)*. The angles were determined to be φ = 49° and θ = −17.31°.

4. Discussion

The 2D projection images in Figure 13 yield intriguing results. First, if we compare the first three (A, C, B) X-Y projections, we can see that the first two are close to the Parker-spiral

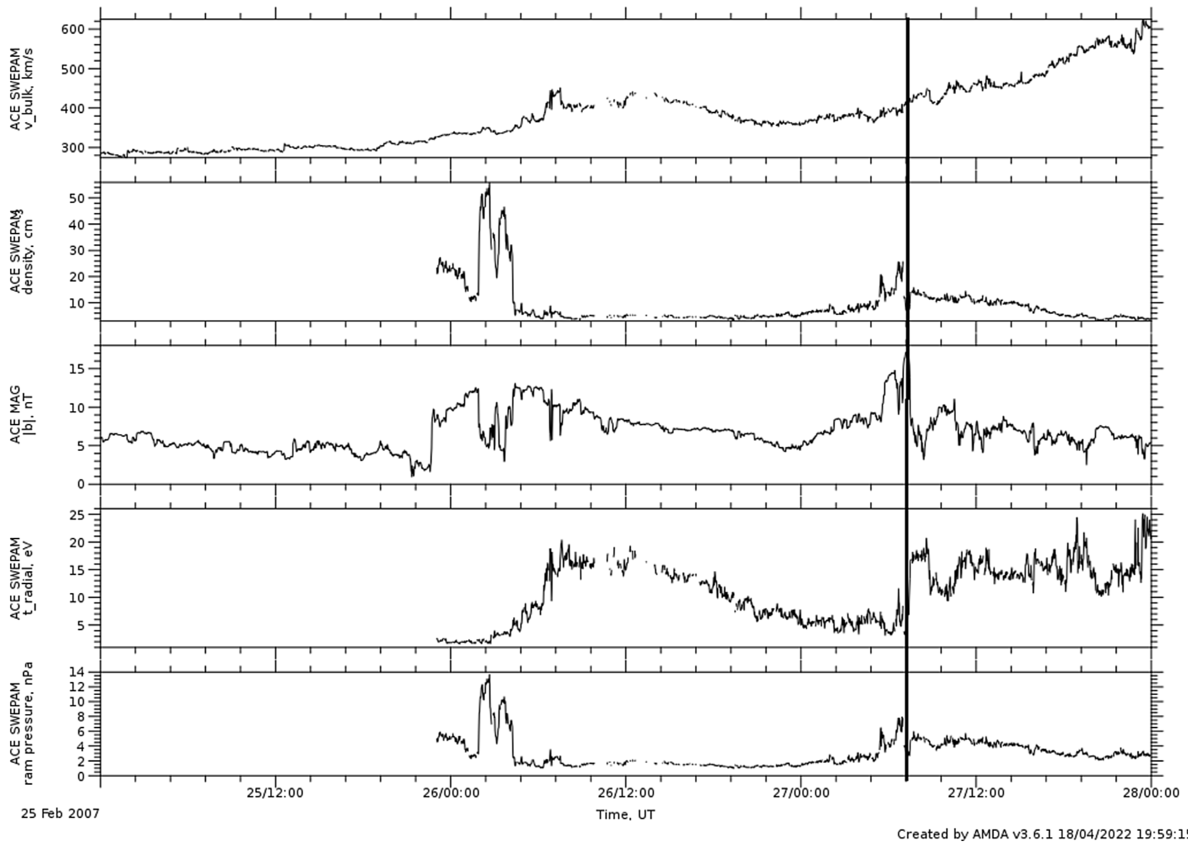

Figure 9. Similar to Figure 3, but for the time period between 25 and 28th February 2007 (D).

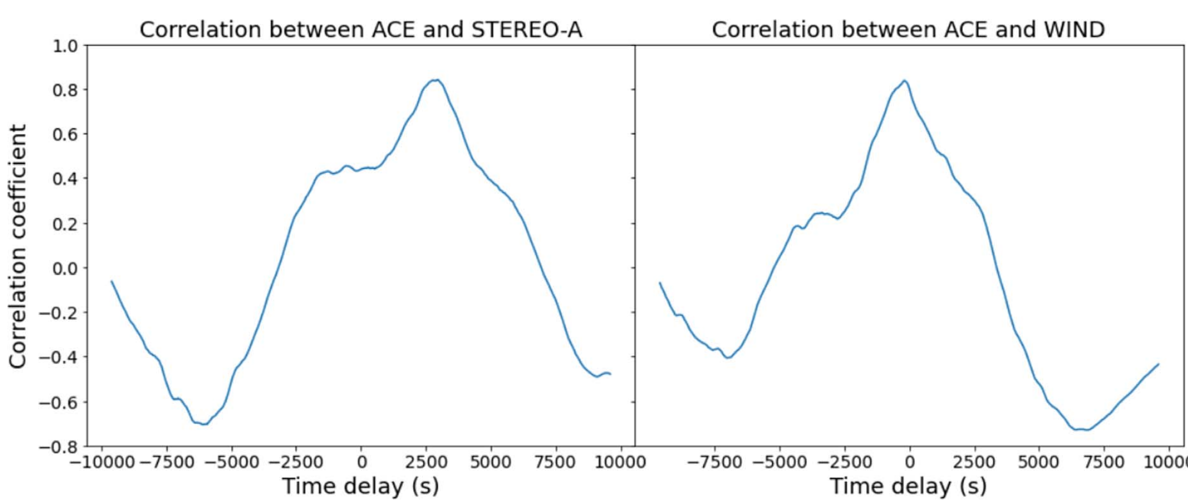

Figure 10. Correlation functions of ACE-STEREO-A and ACE-WIND spacecraft total magnetic field data. This is an excerpt from Figure 2.

direction that we would expect at 1 AU, namely 45°. The third one (B) is considerably off-angle. Chang et al. (2022) show that the distribution of the Parker spiral angle at 1 AU is a double-gaussian, the variation and the peak value of which are changing between solar rotations and with solar activity. For the 2006–2009 period, they obtained peaks at 53.74 and 221.16°, with a variance of 56.66° and 58.08° for the two gaussian distributions. Moreover, Gonzalez-Esparza et al. (2013) studied five CIRs using five space probes (Helios 1, Helios 2, IMP-8, Voyager 1, Voyager 2) from November 1977 to February 1978. They found latitudinal declinations ranging from $-30.7°$ to $38.2°$. Comparing these results to ours, the deviation from the average Parker angle we detected is well within the usual variation. One of the possible reasons for the higher angle is a solar wind velocity difference between the positions of ACE and STEREO-A. Unfortunately, we do not have bulk velocity measurements from STEREO-A for the third event, but for the last one, the velocity is 15% higher at STEREO-A.

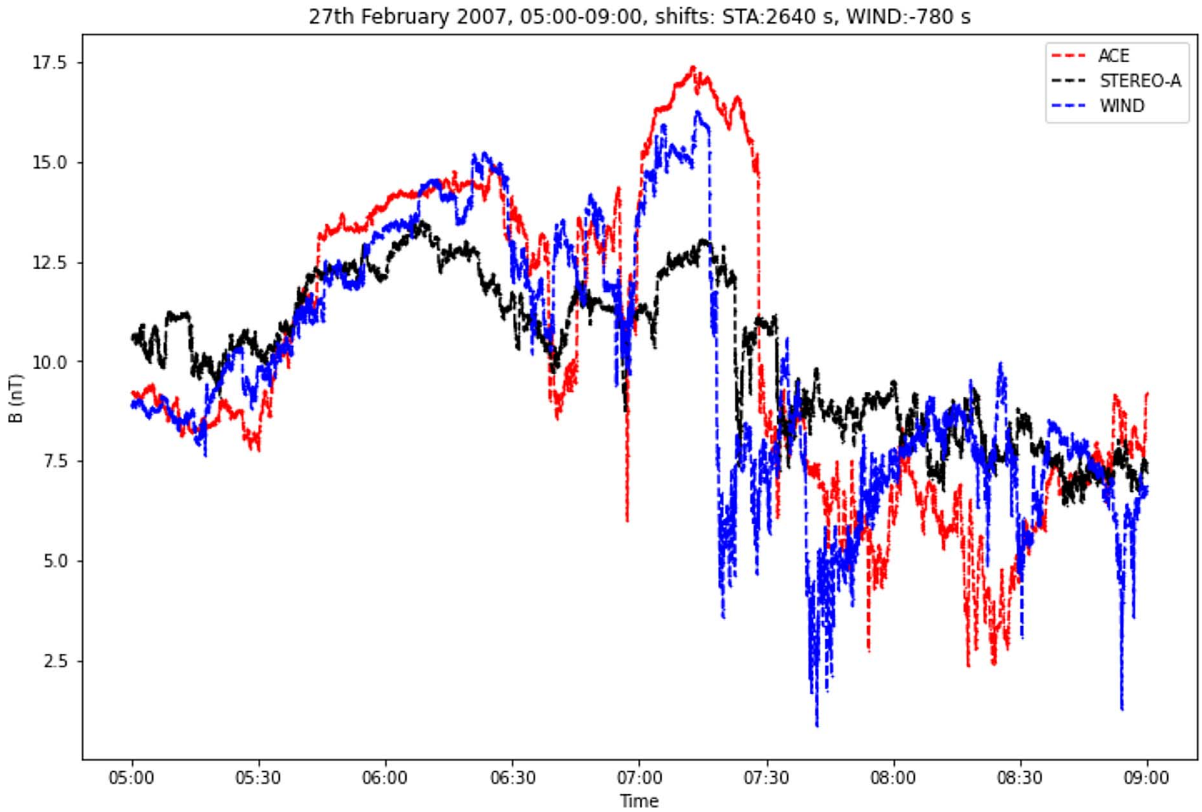

Figure 11. Shifted time series of the total magnetic field measurements for ACE, STEREO-A, and WIND.

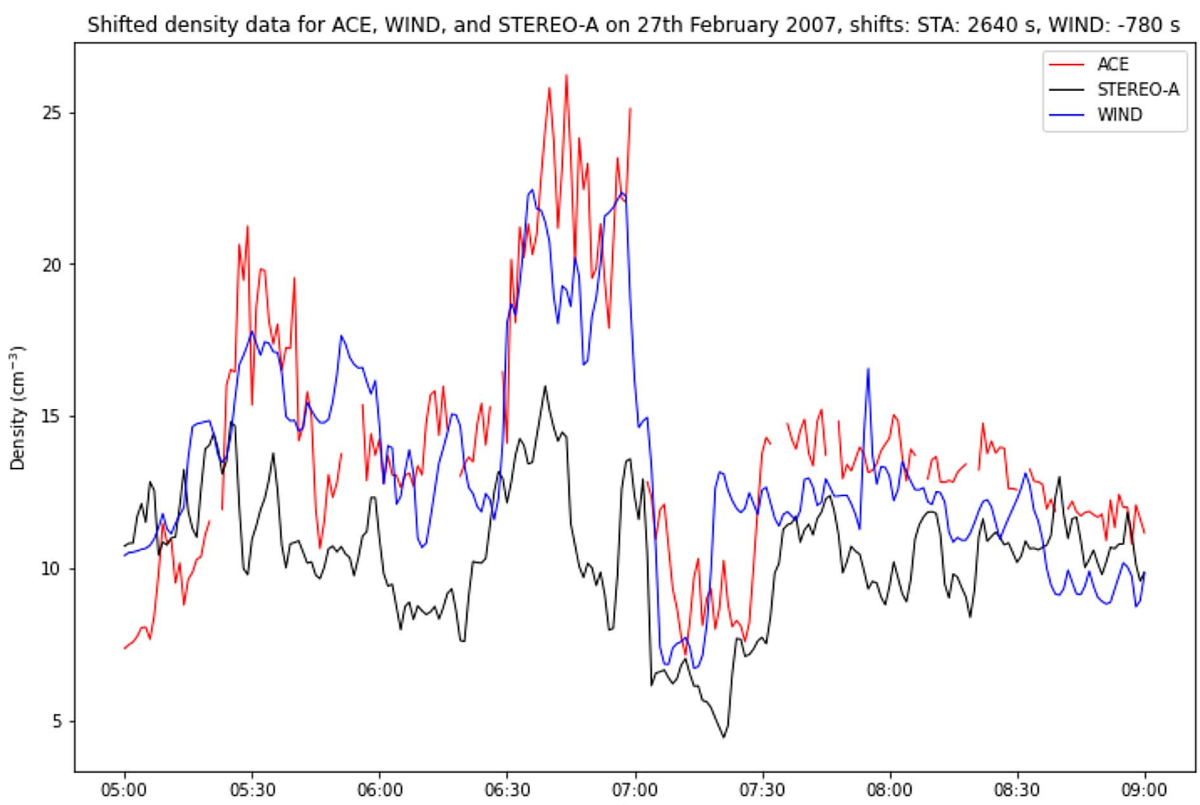

Figure 12. Shifted time series for proton number density measurements of ACE, WIND, and STEREO-A

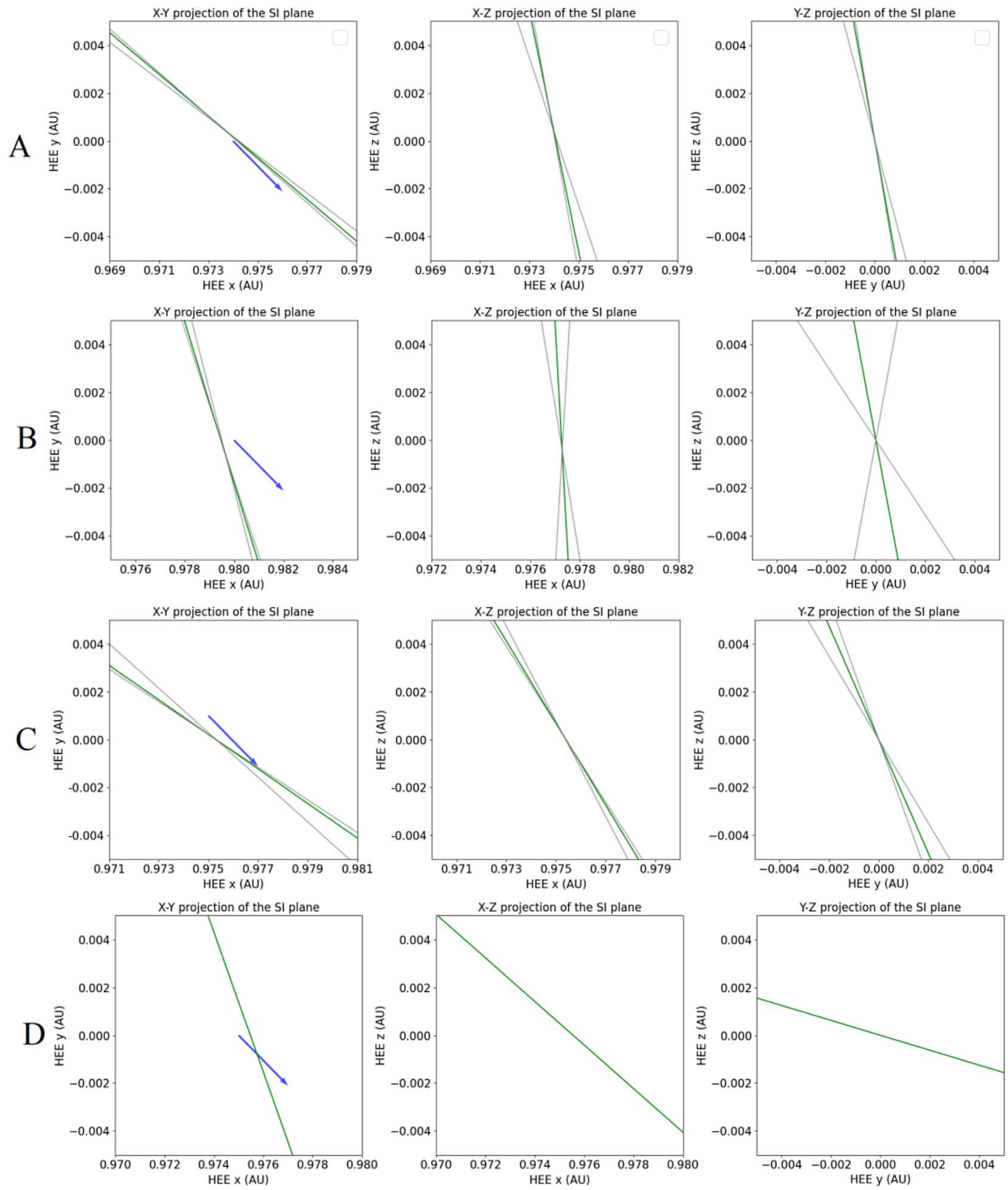

Figure 13. 2D projections of the obtained plane for all four events. The gray lines represent the uncertainty in the obtained plane, and the blue arrow depicts the ideal parker spiral direction.

This could be the reason behind the Parker-spiral angle we detected. Another possibility to be considered is a ripple on the SI surface.

The X–Z projections show a larger tilt for the second event (C), while the first (A) and third (B) is almost vertical and very similar. There is a 28-day long gap between the first (A) and third (B) stream interface, which, together with the resemblance in the X–Z tilt suggests that we see the same CIR after one solar rotation, which explains their similarity. All three SIs are tilted in such a way that their northern side is closer to the Sun. One possible reason for this is that the fast solar wind streams of these CIRs originate from a coronal hole in the southern hemisphere of the Sun, which is indeed the case according to GONG synoptic coronal hole maps for this time period. Since the solar wind flowing from the unperturbed central region of the southern coronal hole is faster than that flowing from near its edges, the northern part of the SI can lag behind the southern part, which is pushed by a somewhat faster wind. The difference is small thus the SI deviates little from the vertical position. This provides information on the latitudinal gradient of the average solar wind speed integrated from the source surface to the point of measurement for the fast solar wind corresponding to a given coronal hole. As such, it may be a better indicator of the global velocity structure at the source than the local speed measurements loaded with small-scale spatial and temporal fluctuations.

The Y–Z projections are not independent in the linear approximation; the X–Y projections, which tell us how the SI spirals around the Sun, and the X–Z projections, which contain information about the latitudinal structure, completely determine the third projection.

For the fourth CIR (D), the results are inconclusive. Although the X–Y projection bears a likeness to the third event, in the X–Z projection we can see that the plane is clearly off, it has a very large tilt. This, together with the worsening of the correlation between STEREO-A and the other spacecraft, suggest that we reached the limit of our method. Even using density and other measurement data does not allow us to state that such a large tilt is a physical phenomenon. Analyses of the events after February exhibit similar problems. This indicates that the method reached its limit, namely that STEREO-A was already too far away from the other spacecraft at this time for this procedure to work. The distance between STEREO-A and ACE was around 3.5 million km at the time of the fourth event, and it was nearly 2.4 million km at the time of the third event. Considering this, the range between the probes used should be less than 2.5 million km for this method to be effective. On the other hand, the separation should be at least a few tens of thousands of km for the relative error of the position determination to be small. Fortunately, we know many such constellations, for example, the DSCOVR, ACE, and WIND spacecraft orbiting the L1 point of Earth, and thus it is possible to use our method to study the structure of CIRs further.

5. Conclusions

In this article, we demonstrated an effective, yet numerically undemanding procedure to analyze the three-dimensional structure of Stream Interfaces of CIRs. We were able to determine the range limit between the spacecraft to be used for the method to work well. As a way of validation, we provided case studies for three events in early 2007. The determined planes generally follow the Parker spiral in the ecliptic, as expected; their off-ecliptic tilt is determined by the position of the source of the high-speed stream. Results for the fourth event are inconclusive because the spatial separation between STEREO-A and the other two spacecraft was too large. The method presents a tool for further studies of the orientation of Stream Interface in CIRs.

Acknowledgements. The authors are grateful for the STEREO, ACE, and WIND spacecraft and instrument teams. Part of the data analysis was performed with the AMDA science analysis system provided by the Centre de Données de la Physique des Plasmas (CDPP) supported by CNRS, CNES, Observatoire de Paris, and Université Paul Sabatier, Toulouse. This work was supported by the NKFIH/OTKA FK128548 project. The editor thanks two anonymous reviewers for their assistance in evaluating this paper.

Data availability

AMDA: http://amda.irap.omp.eu/
STEREO-A positions obtained from: https://izw1.caltech.edu/STEREO/docs/position.html

Supplementary materials

The supplementary information of this article is available at https://www.swsc-journal.org/10.1051/swsc/2023011/olm.

Supplementary Video: In this video, we can see the calculated plane and the positions of the spaceprobe in 3D for event A. Positions of ACE (black), STEREO-A (red), and WIND (blue) at the time of Event A. Triangles depict the positions obtained after shifting with the time delay. The grey shaded area represents the calculated plane. The Sun is in the (0, 0, 0) point of the coordinate system.

References

Acuña MH, Curtis D, Scheifele JL, Russell CT, Schroeder P, Szabo A, Luhmann JG. 2008. The STEREO/IMPACT magnetic field experiment. *Space Sci Rev* **136**: 203–226. https://doi.org/10.1007/s11214-007-9259-2.

Bagashvili S, Shergelashvili B, Japaridze R, Chargeishvili B, Kosovichev A, et al. 2017. Statistical properties of coronal hole rotation rates: Are they linked to the solar interior? *A&A* **603**: A134. https://doi.org/10.1051/0004-6361/201630377.

Bowley AL. 1928. The standard deviation of the correlation coefficient. *J Am Stat Assoc* **23(161)**: 31–34. https://doi.org/10.2307/2277400.

Burlaga LF. 1974. Interplanetary Stream Interface. *J Geophys Res* **79**: 3717. https://doi.org/10.1029/JA079i025p03717.

Chang Q, Xu X, Wang X, Ye Y, Xu Q, et al. 2022. The solar wind parker spiral angle distributions and variations at 1 au. *Astrophys J* **931**: 2. https://doi.org/10.3847/1538-4357/ac6bf3.

Galvin AB, Kistler LM, Popecki MA, et al. 2008. The Plasma and Suprathermal Ion Composition (PLASTIC) Investigation on the STEREO Observatories. *Space Sci Rev* **136**: 437–486. https://doi.org/10.1007/s11214-007-9296-x.

Génot V, Budnik E, Jacquey C, Bouchemit M, Renard B, et al. 2021. Automated Multi-Dataset Analysis (AMDA): An on-line database and analysis tool for heliospheric and planetary plasma data. *Planet Space Sci* **201**: 105214. https://doi.org/10.1016/j.pss.2021.105214.

Gonzalez-Esparza JA, Romero-Hernandez E, Riley P. 2013. Study of corotating interaction regions in the ascending phase of the solar cycle: Multi-spacecraft observations. *Sol Phys* **285**: 201–216. https://doi.org/10.1007/s11207-013-0282-z.

Gosling JT, Pizzo VJ. 1999. Formation and evolution of corotating interaction regions and their three dimensional structure. *Space Sci Rev* **89**: 21–52. https://doi.org/10.1023/A:1005291711900.

Hapgood MA. 1992. Space physics coordinate transformations: A user guide. *Planet Space Sci* **40(5)**: 711–717. https://doi.org/10.1016/0032-0633(92)90012-D.

Harten R, Clark K. 1995. The design features of the GGS wind and polar spacecraft. *Space Sci Rev* **71**: 23–40. https://doi.org/10.1007/BF00751324.

Kaiser ML, Kucera TA, Davila JM, St. Cyr OC, Guhathakurta M, Christian E. 2008. The STEREO mission: An introduction. *Space Sci Rev* **136**: 5–16. https://doi.org/10.1007/s11214-007-9277-0.

Kilpua E, Liewer P, Farrugia C, Luhmann J, Möstl C, et al. 2009. Multispacecraft observations of magnetic clouds and their solar origins between 19 and 23 May 2007. *Solar Phys* **254**: 325–344. https//doi.org/10.1007/s11207-008-9300-y.

Lepping RP, Acũna MH, Burlaga LF, Farrell WM, Slavin JA, et al. 1995. The WIND magnetic field investigation. *Space Sci Rev* **71**: 207–229. https//doi.org/10.1007/BF00751330.

Mason GM, Desai MI, Mall U, Korth A, Bucik R, von Rosenvinge TT, Simunac KD. 2009. In situ observations of CIRs on STEREO, Wind, and ACE During 2007–2008. *Solar Phys* **256**: 393–408. https://doi.org/10.1007/s11207-009-9367-0.

McComas DJ, Bame SJ, Barker P, Feldman WC, Phillips JL, Riley P, Griffee JW. 1998. Solar wind electron proton alpha monitor (SWEPAM) for the advanced composition explorer. *Space Sci Rev* **86**: 563–612. https://doi.org/10.1023/A:1005040232597.

Müller-Mellin R, Böttcher S, Falenski J, Rode E, Duvet L, Sanderson T, Butler B, Johlander B, Smit H. 2008. The Solar Electron and Proton Telescope for the STEREO Mission. *Space Sci Rev* **136(1–4)**: 363–389. https://doi.org/10.1007/s11214-007-9204-4.

Neugebauer M. 1999. The three-dimensional solar wind at solar activity minimum. *Rev Geophys* **37(1)**: 107–126.

Ogilvie KW, Chornay DJ, Fritzenreiter RJ, Hunsaker F, Keller J, et al. 1995. SWE, a comprehensive plasma instrument for the WIND spacecraft. *Space Sci Rev* **71**: 55–77. https://doi.org/10.1007/BF00751326.

Opitz A, Sauvaud J-A, Klassen A, Gómez-Herrero R, Bučík R, et al. 2014. Solar wind control of the terrestrial magnetotail as seen by STEREO. *J Geophys Res* **119**: 6342–6355. https://doi.org/10.1002/2014JA019988.

Phillips JL, Bame SJ, Feldman WC, Gosling JT, Hammond CM, et al. 1995. Ulysses solar wind plasma observations at high southerly latitudes. *Science* **268**: 1030–1033.

Richardson IG. 2018. Solar wind stream interaction regions throughout the heliosphere. *Living Rev Sol Phys* **15**: 1. https://doi.org/10.1007/s41116-017-0011-z.

Russell CT, Mellott MM, Smith EJ, King JH. 1983. Multiple spacecraft observations of interplanetary shocks: Four spacecraft determination of shock normals. *J Geophys Res* **88(A6)**: 4739–4748. https://doi.org/10.1029/JA088iA06p04739.

Sauvaud JA, Larson D, Aoustin C, Curtis D, Médale JL, et al. 2008. The IMPACT solar wind electron analyzer (SWEA). In: *The STEREO mission*. Russell CT, (Ed.) Springer, New York, NY, 227–239. ISBN 978-0-387-09649-0. https://doi.org/10.1007/978-0-387-09649-0_9.

Simunac KDC, Kistler LM, Galvin AB, Lee MA, Popecki MA, et al. 2009. In situ observations of solar wind stream interface evolution. *Solar Phys* **259**: 323–344. https://doi.org/10.1007/s11207-009-9393-y.

Smith CW, L'Heureux J, Ness N, Acuña M, Burlaga LF, Scheifele J. 1998. The ace magnetic fields experiment. *Space Sci Rev* **86**: 613–632. https://doi.org/10.1023/A:1005092216668.

Stone EC, Frandsen AM, Mewaldt RA, Christian ER, Margolies D, Ormes JF, Snow F. 1998. The advanced composition explorer. *Space Sci Rev* **86**: 1–22. https://doi.org/10.1023/A:1005082526237.

Szabo A. 2005. Multi-spacecraft observations of interplanetary shocks. In: *The Physics of Collisionless Shocks: 4th Annual IGPP International Astrophysics Conference*, *AIP Conference Series*, vol. **781**, Li G, Zank GP, Russell CT, (Eds.) American Institute of Physics, New York. pp. 37–41. https://doi.org/10.1063/1.2032672

Wang Y-M, Sheeley NR, Socker DG, Howard RA, Rich NB. 2000. The dynamical nature of coronal streamers. *J Geophys Res* **105(A11)**: 25133–25142. https://doi.org/10.1029/2000JA000149.

Cite this article as: Koban G, Opitz A, Biro N & Nemeth Z. 2023. Orientation of the stream interface in CIRs. *J. Space Weather Space Clim*. **13**, 14. https://doi.org/10.1051/swsc/2023011.